

Data-Driven Linear Complexity Low-Rank Approximation of General Kernel Matrices: A Geometric Approach

Difeng Cai* Edmond Chow † Yuanzhe Xi*

Abstract

A general, *rectangular* kernel matrix may be defined as $K_{ij} = \kappa(x_i, y_j)$ where $\kappa(x, y)$ is a kernel function and where $X = \{x_i\}_{i=1}^m$ and $Y = \{y_i\}_{i=1}^n$ are two sets of points. In this paper, we seek a low-rank approximation to a kernel matrix where the sets of points X and Y are large and are not well-separated (e.g., the points in X and Y may be “intermingled”). Such rectangular kernel matrices may arise, for example, in Gaussian process regression where X corresponds to the training data and Y corresponds to the test data. In this case, the points are often high-dimensional. Since the point sets are large, we must exploit the fact that the matrix arises from a kernel function, and avoid forming the matrix, and thus ruling out most algebraic techniques. In particular, we seek methods that can scale linearly, i.e., with computational complexity $O(m)$ or $O(n)$ for a fixed accuracy or rank. The main idea in this paper is to *geometrically* select appropriate subsets of points to construct a low rank approximation. An analysis in this paper guides how this selection should be performed.

1 Introduction

Given a function $\kappa(x, y)$ and two sets of points $X = \{x_i\}_{i=1}^m$ and $Y = \{y_i\}_{i=1}^n$, the m -by- n matrix with entries

$$K_{ij} = \kappa(x_i, y_j), \quad x_i \in X, \quad y_j \in Y \quad (1)$$

and denoted by K_{XY} is called a *kernel matrix* and $\kappa(x, y)$ is called a kernel function. Kernel matrices associated with various kernel functions arise in diverse computations such as those involving integral equations [38, 37, 4, 46, 19], N -body simulations [5, 29], Gaussian processes [9, 22], and others [50, 31, 36, 34, 35].

One frequently encounters the problem of finding a low-rank factorization, exactly or approximately, of a kernel matrix. We first note that algebraic techniques such as the singular value decomposition and some pseudoskeleton [49, 27, 28, 23] and CUR decompositions [41, 3] do not take advantage of the fact that a matrix is a *kernel* matrix. We further note that when the kernel function $\kappa(x, y)$ is smooth (but possibly singular at $x = y$) and the datasets X, Y are well-separated, then the corresponding kernel matrix K_{XY} generally has low numerical rank and there exists a variety of efficient methods for finding the low-rank approximation (e.g., degenerate approximations of the kernel function [46, 29, 33, 2, 48, 11, 16] and proxy point methods [26, 54]).

In this paper, we seek a low-rank approximation to a kernel matrix where the sets of points X and Y are large and are not well-separated (e.g., the points in X and Y may be “intermingled”). Since the point sets are large, we must exploit the fact that the matrix arises from a kernel function, and avoid forming the matrix, and thus ruling out most algebraic techniques. In particular, we seek methods that can scale linearly, i.e., with computational complexity $O(m)$ or $O(n)$ for a fixed accuracy or rank. Such kernel matrices arise, for example, in Gaussian process regression where

*Department of Mathematics, Emory University, Atlanta, GA 30322 (dcai7@emory.edu, yxi26@emory.edu). The research of Difeng Cai and Yuanzhe Xi is supported by NSF award OAC 2003720.

†School of Computational Science and Engineering, Georgia Institute of Technology, Atlanta, GA 30332 (echow@cc.gatech.edu). The research of Edmond Chow is supported by NSF award OAC 2003683.

X corresponds to the training data and Y corresponds to the test data. In this case, the points are often high-dimensional, which also rules out the use of any existing methods (e.g., degenerate approximations and proxy point methods) that are limited by the curse of dimensionality.

An existing method called adaptive cross approximation (ACA) [7, 8] is often suitable for our case. ACA scales linearly with the number of points. ACA corresponds to a pivoted partial LU factorization and only needs to compute matrix elements used in the partial factorization. However, ACA may fail in some circumstances since it does not perform full pivoting [10, 20]. We will numerically compare our proposed method to ACA later in this paper.

The main idea in this paper is to *geometrically* select a subset of points S_1 in X and/or a subset of points S_2 in Y to construct a low rank approximation. An analysis in this paper guides how this selection should be performed.

We analyze the use of these subsets of points to construct two forms of low-rank factorizations. The first is a two-sided form:

$$K_{XY} \approx K_{XS_2} K_{S_1S_2}^+ K_{S_1Y}, \quad S_1 \subseteq X, \quad S_2 \subseteq Y, \quad (2)$$

where $K_{S_1S_2}^+$ denotes the pseudoinverse of $K_{S_1S_2}$. This form is a CUR decomposition, except that we will treat K_{XY} as a kernel matrix. Note that this form is similar to that of a Nyström factorization, except that a Nyström factorization [53] expects the kernel matrix to be symmetric, with $Y = X$, since eigenvalues of the kernel matrix are implicitly being approximated in the Nyström factorization. The matrix K_{XY} in (2) is rectangular in general.

The second form of low-rank factorization that we study is the one-sided form of the interpolative decomposition [21]:

$$K_{XY} \approx UK_{\mathcal{I}Y}, \quad U = P \begin{bmatrix} I \\ G \end{bmatrix}, \quad (3)$$

where $\mathcal{I} \subseteq X$, P is a permutation matrix, and G is a matrix whose max-norm is bounded by a prescribed constant larger than 1. This form can be computed algebraically with the strong rank-revealing QR factorization [30], but that would require K_{XY} to be formed explicitly. Instead, it is common to algebraically compute the interpolative decomposition of the smaller matrix

$$K_{XS_2} \approx UK_{\mathcal{I}S_2}, \quad U = P \begin{bmatrix} I \\ G \end{bmatrix}, \quad (4)$$

where $S_2 \subseteq Y$ or S_2 is an entirely different set of points altogether, and then use U and \mathcal{I} computed in (4) for the approximation (3). Examples of this approach can be found in [10, 26, 20]. In these approaches, the choice of S_2 is made analytically (e.g., Chebyshev points [10, 20] or proxy surface points [26]) or algebraically (e.g., ACA) [10]. In this paper, for the one-sided approximation (3), we will analyze a *geometric* choice of the subset S_2 . After S_2 is chosen, the subset \mathcal{I} is selected by the algebraic interpolative decomposition via strong rank-revealing QR factorization.

This paper will show that the low-rank approximation error in the maximum norm depends on the quantities δ_{X,S_1} and/or δ_{Y,S_2} , where

$$\delta_{Z,S} := \max_{x \in Z} \text{dist}(x, S)$$

measures the closeness between Z and S . In order for δ_{X,S_1} (or δ_{Y,S_2}) to be small, points in S_1 (or S_2) should be close to as many points in X (or Y) as possible. This implies that selecting sample points that are evenly distributed over the entire dataset can yield better approximations than, for example, choosing clustered points in small regions that fail to capture the geometry of the entire dataset. A similar geometric selection can be used in a version of skeletonized interpolation [55] but has only been studied in the case of well-separated sets of points.

Several known methods can be used to select $O(1)$ sample points that are evenly distributed over a dataset with a complexity that scales *linearly* with the size of the dataset. For example, *farthest point sampling* (FPS) [24] constructs a subset S of X by first initializing S with one point and then sequentially adding the point in X not in S that is farthest from the current points in S . The complexity for selecting r samples from n points in \mathbb{R}^d is $O(dr^2n)$. FPS produces highly evenly distributed samples and is often used in mesh generation [45], computer graphics [47], etc.,

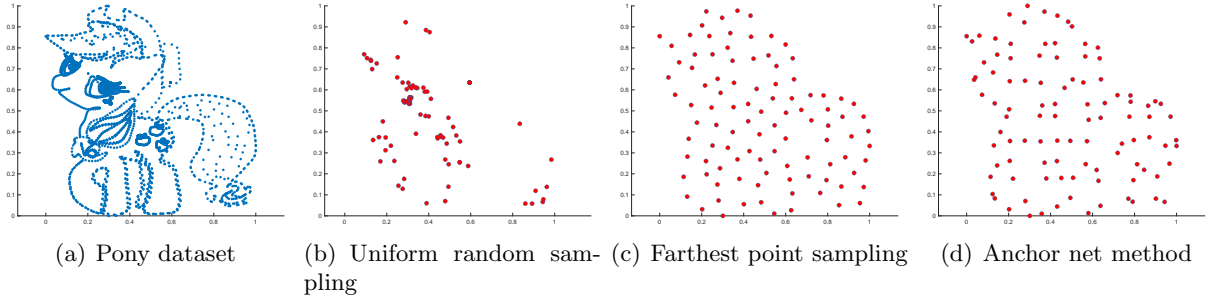


Figure 1: Different geometric selection schemes for the Pony dataset.

but primarily where the data are at most three dimensional. It has not previously been used for the low-rank compression of matrices or applied to high dimensional datasets. Computationally, for high dimensional datasets, FPS can be potentially slow in practice due to its sequential nature. One can combine FPS with uniform random sampling for faster speed, for example, by generating approximately 20% of samples using FPS and 80% using uniform random sampling. As will be shown in Section 4.2, the resulting *mixed method* tends to yield an approximation that is less accurate than FPS and more accurate than random sampling.

Another method for selecting evenly distributed sample points is the *anchor net method* [18]. This method was proposed for the efficient generation of landmark points for Nyström approximations such that the resulting approximation is accurate and numerically stable. It leverages discrepancy theory to generate evenly-spaced samples and was shown in [18] to achieve better accuracy and robustness than uniform random sampling and k -means clustering for low-rank approximations. The anchor net method has the optimal complexity $O(drn)$ for selecting r points from n points in \mathbb{R}^d and is efficient for a wide range of problems from low to high dimensions. However, the anchor net method has only been used for approximating symmetric kernel matrices and its performance for approximating general rectangular kernel matrices is as yet unknown.

Figure 1 shows the 100 samples obtained from FPS and the anchor net method for a highly irregular dataset in two dimensions. Results for uniform random sampling is also shown, which does not generally produce a uniform distribution of points over the data.

In summary, we seek a linear complexity low-rank factorization approach for kernel matrices where the points may be intermingled and the points may be high-dimensional. Some low-rank approximation techniques are matrix-based (e.g., ACA) and don't rely on knowing the specific kernel function or sets of points, except for assuming that the kernel function is smooth and gives rise to a kernel matrix K_{XY} that is low rank. Other techniques only need knowledge of the kernel function and bounding boxes for the sets of points, and do not depend on the points themselves when selecting the set S_2 in (4), for example. The method we propose is based on the sets X and Y and is independent of the kernel function. We thus call our method a *data-driven* method. By choosing S_2 to be existing points rather than a new set of points that sample possibly high-dimensional space, the data-driven method is not limited by the curse of dimensionality.

Our proposed method relies on the geometric selection of the subsets $S_1 \subseteq X$ and/or $S_2 \subseteq Y$. We address the following questions: (1) how does the data selection affect the low-rank approximation error? (2) given two subsets with equal numbers of points, how can one tell which one leads to a more accurate low-rank approximation? (3) how can one perform the desired data selection efficiently?

The rest of the paper is organized as follows. Section 2 proposes the data-driven approach for efficiently computing the *two-sided* factorization (2). Section 3 similarly considers the *one-sided* factorization (3). We will show that the one-sided factorization is more stable than the two-sided factorization. The two-sided factorization, however, is slightly cheaper to compute than the one-sided factorization. The results of numerical experiments are presented in Section 4, and a conclusion given in Section 5. Unless otherwise stated, all norms used in this paper are the 2-norm, denoted by $\|\cdot\|$. The Euclidean distance between $x, y \in \mathbb{R}^d$ is denoted by $|x - y|$.

2 Two-sided low-rank kernel matrix approximation

This section analyzes the data-driven geometric approach for the two-sided low-rank approximation (2).

2.1 Algorithm

The two-sided factorization (2) can be computed immediately once the subsets $S_1 \subseteq X$ and $S_2 \subseteq Y$ are determined. The subsets can be computed in linear time with suitable geometric selection schemes. The full algorithm is given in Algorithm 1. Depending on the specific geometric selection scheme, the total complexity of Algorithm 1 is $O(dr(m+n))$ for uniform random sampling and the anchor net method, or $O(dr^2(m+n))$ for farthest point sampling, where $r = \max(r_1, r_2)$ denotes the maximum sample size. The choice of subsets has a strong impact on the low-rank approximation accuracy, robustness of the algorithm, as well as numerical stability, and thus the subset has to be chosen judiciously. Theoretical guidance on geometric selection is provided in Section 2.2 via analyzing the approximation error of the two-sided factorization. Experiments in Section 4.2 show that different geometric selections can yield dramatically different results for approximating the kernel matrix, with FPS and the anchor net method yielding the best results, which is consistent with our analysis.

Algorithm 1 *Data-driven two-sided compression of K_{XY} with two sets of points X, Y*

Input: Datasets $X = \{x_1, \dots, x_m\}$, $Y = \{y_1, \dots, y_n\} \subset \mathbb{R}^d$, kernel function κ , numbers of sample points r_1, r_2 for X, Y , respectively

Output: Approximation $K_{XY} \approx K_{XS_2} K_{S_1 S_2}^+ K_{S_1 Y}$ with $\text{card}(S_1) = r_1$, $\text{card}(S_2) = r_2$

- 1: Apply a linear complexity geometric selection algorithm to X and Y to generate r_1 and r_2 samples $S_1 \subseteq X$ and $S_2 \subseteq Y$, respectively
 - 2: **return** $K_{XS_2}, K_{S_1 S_2}, K_{S_1 Y}$
-

2.2 Error analysis for two-sided approximation

The goal of this section is to derive an error estimate of the two-sided approximation that is able to provide a straightforward geometric understanding of how the subsets S_1, S_2 affect the approximation accuracy. This analysis is independent of how the subsets S_1, S_2 are selected in Algorithm 1. To prepare for the derivation of the geometric estimates, in Section 2.2.1, we derive error bounds involving only submatrices of K_{XY} . The geometric estimates are presented in Section 2.2.2.

2.2.1 Algebraic preparation

In order to estimate for the approximation error of (2) for arbitrary subsets $S_1 \subseteq X$ and $S_2 \subseteq Y$, we first review one lemma from [18, Lemma 3.1], which is stated below.

Lemma 2.1. *Assume A is an m -by- n matrix, $\alpha, \hat{\alpha}$ are m -by-1 vectors and $\beta, \hat{\beta}$ are n -by-1 vectors. Define $\epsilon_1 := \|\hat{\alpha} - \alpha\|$ and $\epsilon_2 := \|\hat{\beta} - \beta\|$. Then*

$$\left| \hat{\alpha}^T A \hat{\beta} - \alpha^T A \beta \right| \leq \|\alpha^T A\| \cdot \epsilon_2 + \|A\beta\| \cdot \epsilon_1 + \|A\| \cdot \epsilon_1 \epsilon_2. \quad (5)$$

In the next theorem, we derive the estimate for the entrywise approximation error of (2) at an arbitrary pair of points (x, y) . This can be viewed as an error estimate for the “*algebraic*” separable approximation to the kernel function $\kappa(x, y)$.

Theorem 2.1. Consider finite sets $X, Y \subset \mathbb{R}^d$ and a kernel function $\kappa(x, y)$ defined on $X \times Y$. For any non-empty subsets $S_1 \subseteq X$ and $S_2 \subseteq Y$, the entrywise error of the approximation in (2) satisfies

$$|\kappa(x, y) - K_{xS_2} K_{S_1S_2}^+ K_{S_1y}| \leq \min_{\substack{u \in S_1 \\ v \in S_2}} (|\kappa(x, y) - \kappa(u, v)| + \epsilon_1 + \epsilon_2 + \|K_{S_1S_2}^+\| \epsilon_1 \epsilon_2), \quad (6)$$

where $\epsilon_1 = \|K_{xS_2} - K_{uS_2}\|$ and $\epsilon_2 = \|K_{S_1y} - K_{S_1v}\|$.

Proof. Since $K_{S_1S_2} K_{S_1S_2}^+ K_{S_1S_2} = K_{S_1S_2}$, we have $\forall u \in S_1, v \in S_2$

$$\kappa(u, v) = K_{uS_2} K_{S_1S_2}^+ K_{S_1v}. \quad (7)$$

For any $x \in X, y \in Y, u \in S_1, v \in S_2$, define the column vectors

$$\alpha := K_{uS_2}^T, \quad \hat{\alpha} := K_{xS_2}^T, \quad \beta := K_{S_1v}, \quad \hat{\beta} := K_{S_1y}.$$

Then it is easy to see that $\epsilon_1 = \|\hat{\alpha} - \alpha\|$ and $\epsilon_2 = \|\hat{\beta} - \beta\|$. With (7), we obtain

$$\kappa(x, y) - K_{xS_2} K_{S_1S_2}^+ K_{S_1y} = \kappa(x, y) - \hat{\alpha}^T K_{S_1S_2}^+ \hat{\beta} = (\kappa(x, y) - \kappa(u, v)) + (\alpha^T K_{S_1S_2}^+ \beta - \hat{\alpha}^T K_{S_1S_2}^+ \hat{\beta}), \quad (8)$$

for any $u \in S_1, v \in S_2$. According to Lemma 2.1, we get

$$\begin{aligned} \left| \hat{\alpha}^T K_{S_1S_2}^+ \hat{\beta} - \alpha^T K_{S_1S_2}^+ \beta \right| &\leq \|\alpha^T K_{S_1S_2}^+\| \epsilon_2 + \|K_{S_1S_2}^+ \beta\| \epsilon_1 + \|K_{S_1S_2}^+\| \epsilon_1 \epsilon_2 \\ &\leq \epsilon_2 + \epsilon_1 + \|K_{S_1S_2}^+\| \epsilon_1 \epsilon_2. \end{aligned} \quad (9)$$

The last inequality in (9) follows from the fact that $\alpha^T K_{S_1S_2}^+ = K_{uS_2} K_{S_1S_2}^+$ is a row in $K_{S_1S_2} K_{S_1S_2}^+$ and $K_{S_1S_2}^+ \beta = K_{S_1S_2}^+ K_{S_1v}$ is a column in $K_{S_1S_2}^+ K_{S_1S_2}$, and meanwhile

$$\|K_{S_1S_2} K_{S_1S_2}^+\| = \|K_{S_1S_2}^+ K_{S_1S_2}\| = 1.$$

We see from (8) and (9) that

$$\left| \kappa(x, y) - \hat{\alpha}^T K_{S_1S_2}^+ \hat{\beta} \right| \leq |\kappa(x, y) - \kappa(u, v)| + \epsilon_1 + \epsilon_2 + \|K_{S_1S_2}^+\| \epsilon_1 \epsilon_2, \quad \forall u \in S_1, v \in S_2. \quad (10)$$

Minimizing the upper bound in (10) over all $u \in S_1, v \in S_2$ yields (6), which completes the proof. \square

The entrywise estimate in Theorem 2.1 immediately leads to a matrix max norm estimate, which is proved in the next theorem.

Theorem 2.2. Consider finite sets $X, Y \subset \mathbb{R}^d$ and kernel function $\kappa(x, y)$ defined on $X \times Y$. For any non-empty subsets $S_1 \subseteq X$ and $S_2 \subseteq Y$, denote by $\mathcal{X} = X \times Y, \mathcal{S} = S_1 \times S_2$. Then the approximation in (2) satisfies the following estimate

$$\|K_{\mathcal{X}\mathcal{Y}} - K_{XS_2} K_{S_1S_2}^+ K_{S_1Y}\|_{\max} \leq \max_{\substack{x \in X \\ y \in Y}} \min_{\substack{u \in S_1 \\ v \in S_2}} (|\kappa(x, y) - \kappa(u, v)| + \epsilon_1 + \epsilon_2 + \|K_{S_1S_2}^+\| \epsilon_1 \epsilon_2), \quad (11)$$

where $\epsilon_1 = \|K_{xS_2} - K_{uS_2}\|$ and $\epsilon_2 = \|K_{S_1y} - K_{S_1v}\|$.

Proof. Taking maximum of both sides of (6) over $x \in X, y \in Y$ yields (11). \square

Theorems 2.1 and 2.2 imply that the bounds will be small if for any point $x \in X$ there is a point $u \in S_1$ nearby and for any point $y \in Y$ there is a point $v \in S_2$ nearby. As a result, Theorems 2.1 and 2.2 indicate that S_1 and S_2 should be evenly distributed inside X and Y in order to achieve a small approximation error. This can be more easily identified when the special case $S_1 = X$ or $S_2 = Y$ is considered.

Corollary 2.1. *Let $X, Y \subset \mathbb{R}^d$ be finite sets and $\kappa(x, y)$ be defined on $X \times Y$. For any non-empty subsets $S_1 \subseteq X$ and $S_2 \subseteq Y$, the following estimates hold*

$$\begin{aligned} \left\| K_{XY} - Q_{XS_2}^\dagger K_{XY} \right\|_{\max} &\leq \max_{\substack{x \in X \\ y \in Y}} \min_{v \in S_2} (|\kappa(x, y) - \kappa(x, v)| + \|K_{Xy} - K_{Xv}\|), \\ \left\| K_{XY} - K_{XY} Q_{S_1Y}^- \right\|_{\max} &\leq \max_{\substack{x \in X \\ y \in Y}} \min_{u \in S_1} (|\kappa(x, y) - \kappa(u, y)| + \|K_{xY} - K_{uY}\|), \end{aligned} \quad (12)$$

where $Q_{XS_2}^\dagger := K_{XS_2} K_{XS_2}^+$, $Q_{S_1Y}^- := K_{S_1Y}^+ K_{S_1Y}$.

Proof. We only show the first inequality in (12) and the second one can be proved in a similar fashion. Note that the first inequality in (12) is a special case of (11) with $S_1 = X$. In this case, in the upper bound of (11), the minimum over $u \in X$ is no greater than the value achieved by choosing $u = x$. Hence we see that if $S_1 = X$ and $u = x$, then $\epsilon_1 = \|K_{xS_2} - K_{xS_2}\| = 0$ and (11) becomes

$$\left\| K_{XY} - Q_{XS_2}^\dagger K_{XY} \right\|_{\max} \leq \max_{\substack{x \in X \\ y \in Y}} \min_{v \in S_2} (|\kappa(x, y) - \kappa(x, v)| + \|K_{Xy} - K_{Xv}\|),$$

which is the first inequality in (11). \square

Corollary 2.1 further reveals the interconnection between the approximation accuracy and the geometry of sample points. Algebraically, $\left\| K_{XY} - Q_{XS_2}^\dagger K_{XY} \right\|_{\max}$ and $\left\| K_{XY} - K_{XY} Q_{S_1Y}^- \right\|_{\max}$ measure how well K_{XS_2} and K_{S_1Y} capture the column and row spaces of K_{XY} , respectively. Geometrically, the bound on the right-hand side of (12) will be small if S_1 and S_2 are able to capture the global geometry of X and Y , respectively.

2.2.2 Geometric estimates

In the following, we reveal the geometric implication of the error bounds in Theorem 2.2 and Corollary 2.1 with the help of the so-called *discrete Lipschitz constant* as defined below. It is used to derive new error bounds that give a more straightforward interpretation of how the sets of landmark points S_1 and S_2 affect the accuracy of the approximation $K_{XY} \approx K_{XS_1} K_{S_1S_2}^+ K_{S_1Y}$.

Definition 2.1 (Discrete Lipschitz constant). *Let $\kappa(x, y)$ be a function defined on $X \times Y$. Denote $\mathcal{Z} = Z_1 \times Z_2$, $\mathcal{S} = S_1 \times S_2$, $W_1 \times W_2$ as three non-empty subsets of $X \times Y$. The discrete Lipschitz constants of κ associated with these three subsets are defined by*

$$\begin{aligned} L(\mathcal{Z}, \mathcal{S}) &:= \min\{C : |\kappa(x, y) - \kappa(u, v)|^2 \leq C^2(|x - u|^2 + |y - v|^2) \quad \forall (x, y) \in \mathcal{Z}, (u, v) \in \mathcal{S}\}, \\ L(Z_2, S_2)_{W_1} &:= \min\{C : |\kappa(x, y) - \kappa(x, v)|^2 \leq C^2|y - v|^2 \quad \forall x \in W_1, y \in Z_2, v \in S_2\}, \\ L(Z_1, S_1)_{W_2} &:= \min\{C : |\kappa(x, y) - \kappa(u, y)|^2 \leq C^2|x - u|^2 \quad \forall y \in W_2, x \in Z_1, u \in S_1\}. \end{aligned} \quad (13)$$

Since X, Y are finite sets, each minimum in (13) exists. Note that in general $L(\mathcal{Z}, \mathcal{S})$ is *not* the Lipschitz constant of κ since we do *not* assume κ to be Lipschitz continuous or even defined outside $X \times Y$. If $\kappa(x, y)$ is Lipschitz continuous with Lipschitz constant L , then one can easily see that $L(\mathcal{Z}, \mathcal{S}) \leq L$. Kernels in many applications are not only Lipschitz continuous but also smooth in the domain of interest. For example, in machine learning and statistics, the Gaussian kernel $\exp(-\frac{|x-y|^2}{\sigma^2})$ is smooth; radial basis functions like $\sqrt{1 + |x - y|^2}$ and $(1 + |x - y|^2)^{-1/2}$ are smooth; in potential theory, kernels like $\frac{1}{|x-y|}$ are smooth in $D_1 \times D_2$ with well-separated domains D_1 and D_2 , which is a key assumption in the fast multipole method [46, 29, 48] and hierarchical matrices in general [32, 7, 31, 25].

Using the discrete Lipschitz constant, we can show in the following that the low-rank approximation error bound depends on the geometric quantity

$$\delta_{Z, S} := \max_{x \in Z} \text{dist}(x, S) \quad Z \subseteq X. \quad (14)$$

The quantity $\delta_{Z,S}$ measures the closeness between Z and S . The smaller $\delta_{Z,S}$ is, the ‘‘closer’’ S is to Z . In fact, if $\delta_{Z,S}$ is small, then for any $x \in Z$, there exists a point in S that is close to x , and vice versa.

We can now derive an error bound for (2) in terms of the geometric quantities δ_{X,S_1} , δ_{Y,S_2} for subsets $S_1 \subseteq X$, $S_2 \subseteq Y$, respectively. The result is stated in Theorem 2.3.

Theorem 2.3. *Let $X, Y \subset \mathbb{R}^d$ be finite sets and $\kappa(x, y)$ be a function defined on $X \times Y$. For any non-empty subsets $S_1 \subseteq X$ and $S_2 \subseteq Y$, define $\mathcal{X} = X \times Y$, $\mathcal{S} = S_1 \times S_2$. Then the following estimate holds*

$$\|K_{XY} - K_{XS_2}K_{S_1S_2}^+K_{S_1Y}\|_{\max} \leq C_1\delta_{X,S_1} + C_2\delta_{Y,S_2} + C_3\delta_{X,S_1}\delta_{Y,S_2},$$

where

$$\begin{aligned} C_1 &= L(\mathcal{X}, \mathcal{S}) + \sqrt{r_2}L(X, S_1)_{S_2}, \\ C_2 &= L(\mathcal{X}, \mathcal{S}) + \sqrt{r_1}L(Y, S_2)_{S_1}, \\ C_3 &= \|K_{S_1S_2}^+\| \sqrt{r_1 r_2} L(X, S_1)_{S_2} L(Y, S_2)_{S_1}, \end{aligned} \tag{15}$$

with $r_i = \text{card}(S_i)$.

Proof. The result can be proved using Theorem 2.2 and the definition in (13). First we estimate the terms in the upper bound in Theorem 2.2. The definition of Lipschitz constants in (13) implies that

$$\begin{aligned} |\kappa(x, y) - \kappa(u, v)| &\leq L(\mathcal{X}, \mathcal{S}) (|x - u|^2 + |y - v|^2)^{1/2} \leq L(\mathcal{X}, \mathcal{S}) (|x - u| + |y - v|), \\ \epsilon_1 = \|K_{xS_2} - K_{uS_2}\| &\leq \left(\sum_{v \in S_2} L(X, S_1)_{S_2}^2 |x - u|^2 \right)^{1/2} \leq \sqrt{r_2} L(X, S_1)_{S_2} |x - u|, \\ \epsilon_2 = \|K_{S_1y} - K_{S_1v}\| &\leq \left(\sum_{u \in S_1} L(Y, S_2)_{S_1}^2 |y - v|^2 \right)^{1/2} \leq \sqrt{r_1} L(Y, S_2)_{S_1} |y - v|. \end{aligned} \tag{16}$$

Define C_1, C_2, C_3 as in (15). The estimates in (16), which separate (x, u) and (y, v) into different terms, allow us to organize the upper bound in (11) in terms of $|x - u|$ and $|y - v|$ and deduce that

$$\begin{aligned} &\max_{\substack{x \in X \\ y \in Y}} \min_{\substack{u \in S_1 \\ v \in S_2}} (|\kappa(x, y) - \kappa(u, v)| + \epsilon_1 + \epsilon_2 + \|K_{S_1S_2}^+\| \epsilon_1 \epsilon_2) \\ &\leq \max_{\substack{x \in X \\ y \in Y}} \min_{\substack{u \in S_1 \\ v \in S_2}} (C_1|x - u| + C_2|y - v| + C_3|x - u||y - v|) \\ &= \max_{\substack{x \in X \\ y \in Y}} (C_1 \text{dist}(x, S_1) + C_2 \text{dist}(y, S_2) + C_3 \text{dist}(x, S_1) \text{dist}(y, S_2)) \\ &= C_1 \max_{x \in X} \text{dist}(x, S_1) + C_2 \max_{y \in Y} \text{dist}(y, S_2) + C_3 \max_{x \in X} \text{dist}(x, S_1) \max_{y \in Y} \text{dist}(y, S_2) \\ &= C_1\delta_{X,S_1} + C_2\delta_{Y,S_2} + C_3\delta_{X,S_1}\delta_{Y,S_2}, \end{aligned}$$

which completes the proof in view of Theorem 2.2. \square

The estimate in Theorem 2.3 implies that in order to obtain a good approximation, S_1, S_2 should be chosen such that $\delta_{X,S_1}, \delta_{Y,S_2}$ are small. Geometrically, according to the definition of δ in (14), this means that S_1 and S_2 should represent the geometry of X and Y as much as possible. In the context of integral equations, a recent analytical study [6] also discussed the relationship between the approximation error of adaptive cross approximation (ACA) and the selected subsets measured by the geometric concept of *fill distance* (cf. [40]), which reflects how well the subset spans the computational domain. Both fill distance and δ in (14) provide similar geometric interpretations of the quality of the selected subsets.

The error estimates derived in this section apply to *any* subsets $S_1 \subset X$, $S_2 \subset Y$, regardless of the algorithm used to generate S_1, S_2 . Thus when S_1, S_2 are poorly chosen (i.e. corresponding to poor low-rank approximation), we expect the bounds to reflect the fact that the matrix approximation error is large. This motivates the use of the estimates as indicators to distinguish ‘‘good’’ subsets and ‘‘bad’’ subsets, which will be investigated next in Section 2.3.

2.3 Subset quality indicators

The error bounds in Theorems 2.2 and 2.3 are fully computable and can be used to relate the choice of subset to the low-rank approximation error. Error bounds of this kind often arise in a posteriori error estimates for the numerical solution of partial differential equations using adaptive mesh refinement (AMR). In AMR, an error indicator, usually a computable term in the a posteriori error estimate, is used to indicate the quality of the numerical solution and determine whether further refinement is needed without knowing the exact solution (cf. [56, 51, 52, 12, 14, 15, 1]). Inspired by this philosophy, in low-rank compression methods based on geometric selection, we can use the error estimates to construct *subset quality indicators* for inferring the quality of the selected subsets. For any choice of subset $S_1 \times S_2 \subseteq X \times Y$, we consider the following five subset quality indicators:

$$\begin{aligned} \text{indicator 1} &= \max_{\substack{x \in X \\ y \in Y}} \min_{\substack{u \in S_1 \\ v \in S_2}} |\kappa(x, y) - \kappa(u, v)|, & \text{indicator 2} &= \max_{x \in X} \min_{u \in S_1} \|K_{xS_2} - K_{uS_2}\|, \\ \text{indicator 3} &= \delta_{X, S_1}, & \text{indicator 4} &= \delta_{Y, S_2}, & \text{indicator 5} &= \|K_{S_1 S_2}^+\|. \end{aligned} \quad (17)$$

The first two indicators are related to the upper bound derived in Theorems 2.2, while the last three indicators are from the estimate in Theorem 2.3. The costs for computing the indicators are *not* the same. In fact, assume K_{XY} is m -by- n and there are $O(1)$ points in S_1 and S_2 . The computational complexities for the five indicators in (17) are: $O(mn)$, $O(m)$, $O(m)$, $O(n)$, $O(1)$, respectively. Hence in practice, it is more convenient to use the latter four indicators.

Given different choices of subsets, we present numerical experiments below to demonstrate how to use the subset quality indicators to predict which choice is more likely to yield a better approximation without computing the exact matrix approximation error. The results also underscore the impact of the geometry of the selected subset on the low-rank approximation accuracy. We perform two experiments, one with a rectangular kernel matrix associated with *two* sets of points and the other with a symmetric positive definite kernel matrix associated with *one* set of points.

Experiment 1. We consider the approximation $K_{XY} \approx K_{XS_2} K_{S_1 S_2}^+ K_{S_1 Y}$. The kernel function is chosen as $\kappa(x, y) = \log|x - y|$ and the rectangular kernel matrix K_{XY} is associated with X, Y (illustrated in Figure 2(a)), where X contains 50 points and Y contains 100 points. We consider two choices for $S_1 \times S_2 \subset X \times Y$. Choice 1 generates points S_1, S_2 via random sampling from X, Y . Choice 2 chooses evenly distributed points to form S_1, S_2 . These subsets are shown in Figure 2(b) and Figure 2(c). To determine which choice yields the better approximation, we take the ratio of the respective indicators and compare it to the ratio of the exact matrix approximation errors from the two choices. Namely, we compute

$$\text{ratio-indicator } k = \frac{\text{indicator } k \text{ of Choice 2}}{\text{indicator } k \text{ of Choice 1}}, \quad \text{ratio-error} = \frac{\text{matrix error of Choice 2}}{\text{matrix error of Choice 1}},$$

where the matrix approximation error is measured in max norm. If the ratio-indicator is larger than 1, then the prediction is that Choice 1 is better. Otherwise, the prediction is that Choice 2 is better. We then compare the indicator ratios to the ground truth: the ratio of matrix approximation errors between Choice 2 and Choice 1. If the indicator ratio is consistent with the error ratio, i.e. both larger than 1 or both smaller than 1, then the prediction based on the indicator is correct. The result is shown in Figure 2(d). It is easily seen that, for different approximation ranks, the indicator ratios and the error ratio always stay below the horizontal line $y = 1$. Hence the indicators correctly predict the fact that Choice 2 of subsets yields a better low-rank approximation than Choice 1. Furthermore, note that unlike Choice 1, the points in Choice 2 are evenly distributed over the dataset and thus are expected to yield a better approximation according to the theoretical results in Section 2.2.

Experiment 2. We consider the Gaussian kernel $\kappa(x, y) = \exp(-|x - y|^2/0.09)$ and the symmetric approximation $K_{XX} \approx K_{XS} K_{SS}^+ K_{SX}$, where the dataset X is shown in Figure 3(a). We follow the same choices of subset as in Experiment 1, i.e., Choice 1 selects random samples while Choice 2 selects evenly distributed points. These two choices of subset S are shown in Figure 3(b) and Figure 3(c). We compute the same indicators as in (17), where in this case $Y = X$ and $S_2 = S_1 = S$. The result is shown in Figure 2(d). We see that when the approximation rank is

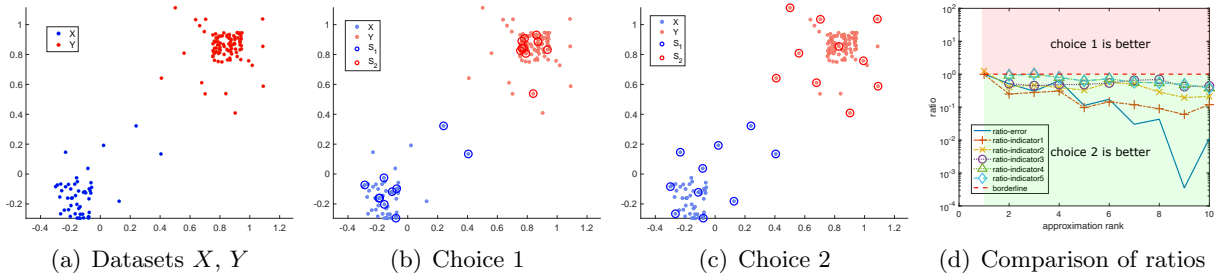


Figure 2: Experiment 1: Predicting the better choice of subsets S_1, S_2 using subset indicators in (17).

larger than 5, all indicator ratios and the error ratio stay below the horizontal line $y = 1$ simultaneously. This implies that Choice 2 yields a better approximation and the indicators give the correct prediction. Again, we see that evenly distributed points yield a better approximation, as discussed in Section 2.2.

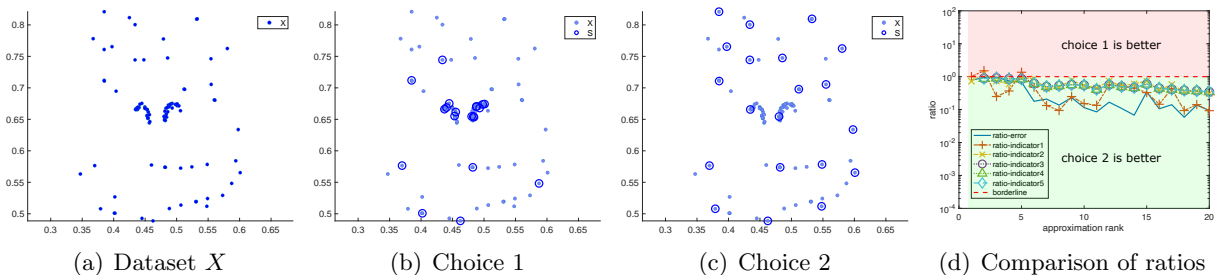


Figure 3: Experiment 2: Predicting the better choice of subset S using subset indicators in (17).

3 One-sided low-rank kernel matrix approximation

This section analyzes the data-driven geometric approach for the one-sided low-rank approximation (3). Compared to the two-sided case, the algorithm in the one-sided case only samples points from one set of points and applies an algebraic compression to postprocess the selected submatrix. Numerical experiments in Section 4 show that the one-sided algorithm is slightly more accurate.

We present the algorithm for the one-sided low-rank approximation in Section 3.1 and provide the error analysis in Section 3.2. The special case of a symmetric kernel matrix K_{XX} with a symmetric kernel $\kappa(x, y) = \kappa(y, x)$ is discussed in Section 3.3.

3.1 Algorithm

The one-sided approximation method consists of two stages. In the first stage, a subset S_2 of Y is selected using a linear complexity geometric selection scheme (Section 1). In the second stage, interpolative decomposition (ID) [21] is applied on K_{XS_2} to obtain the desired approximation (3). The ID property is stated in Proposition 3.1. The ID in Proposition 3.1 can be computed in $O(r^2n)$ complexity for a $n \times r$ matrix with exact rank r .

Proposition 3.1 (Interpolative decomposition). *Let M be an n -by- r matrix with rank r . The interpolative decomposition yields the factorization $M = P \begin{bmatrix} I \\ G \end{bmatrix} M_1$, where P is a permutation matrix, I is an identity matrix, M_1 is the matrix that consists of the first r rows of $P^T M$, and $\|G\|_{\max} \leq s$. Here $s > 1$ is a user-specified constant.*

The full one-sided compression algorithm is summarized in Algorithm 2. Notice that in Step 2 of Algorithm 2, ID is only used to obtain a stable factorization of K_{XS_2} and thus *no* approximation error is introduced.

Algorithm 2 *Data-driven one-sided compression of K_{XY} with two sets of points X, Y*

Input: Datasets $X = \{x_1, \dots, x_m\}$, $Y = \{y_1, \dots, y_n\} \subset \mathbb{R}^d$, kernel function κ , number of sample points r for Y

Output: Low-rank approximation $K_{XY} \approx UK_{\mathcal{I}_1Y}$ in (3)

- 1: Apply a linear complexity geometric selection algorithm to Y to generate r sample points $S_2 \subseteq Y$
 - 2: Apply ID to the m -by- r kernel matrix K_{XS_2} : $K_{XS_2} = P \begin{bmatrix} I \\ G \end{bmatrix} K_{\mathcal{I}_1S_2}$, where $\mathcal{I}_1 \subseteq X$, I is an identity matrix, P is a permutation matrix and $\|G\|_{\max} \leq 2$.
 - 3: Define $U = P \begin{bmatrix} I \\ G \end{bmatrix}$.
 - 4: **return** $U, K_{\mathcal{I}_1Y}$
-

Compared to purely algebraic methods such as LU, QR, rank-revealing QR, and SVD decompositions, Algorithm 2 does not access the full kernel matrix and scales linearly with respect to the data size. Compared to the proxy point methods [26, 54], hybrid cross approximation [10], Algorithm 2 does not require the evaluation of the kernel function outside the given dataset (where the function may not necessarily be defined) and is able to scale to high dimensions. In terms of numerical stability, Algorithm 2 leverages the robustness of algebraic methods to obtain a stable factorization compared to the two-sided approximation. As we shall see in Section 4, despite being more stable and more general, the error-time trade-off of the proposed method can be noticeably better than that of existing methods.

In addition to the factorization $K \approx UK_{\mathcal{I}_1Y}$, a similar one-sided factorization $K \approx K_{X\mathcal{I}_2}V^*$ can be computed by applying Algorithm 2 to K_{XY}^* . That is, we first select a subset from X and then apply ID to obtain a subset $\mathcal{I}_2 \subseteq Y$. In general, one can perform geometric selection on the dataset with more data points so that ID can be applied on a smaller submatrix in order to reduce the total computational cost.

3.2 Complexity and error analysis

In this section, we analyze the complexity and the approximation error of Algorithm 2. First, we show that Algorithm 2 scales as $O(r^2(m+n))$ for obtaining a rank- r approximation to an $m \times n$ kernel matrix.

Theorem 3.1. *Given $X = \{x_i\}_{i=1}^m$, $Y = \{y_i\}_{i=1}^n$ in \mathbb{R}^d and kernel function κ , the complexity of Algorithm 2 to compute a rank- r approximation $K_{XY} \approx UK_{\mathcal{I}_1Y}$ is $O(dr^2(m+n))$.*

Proof. Compressing a set of n points into r points with any scheme in Section 1 has a complexity at most $O(dr^2n)$. The cost of applying ID on a m -by- r matrix K_{XS_2} is $O(r^2m)$. Therefore, the overall complexity of Algorithm 2 is $O(dr^2(m+n))$. \square

Next we analyze the approximation error for $K_{XY} \approx UK_{\mathcal{I}_1Y}$ computed by Algorithm 2. We will see that, different from the two-sided factorization, the error bound for $K_{XY} \approx UK_{\mathcal{I}_1Y}$ does not involve the norm of the pseudoinverse of the matrix.

Theorem 3.2. *Let X and Y be finite sets in \mathbb{R}^d and $\kappa(x, y)$ be defined on $X \times Y$. For any non-empty subset $S \subseteq Y$, let ID of K_{XS} be given by $K_{XS} = UK_{\mathcal{I}S} = P \begin{bmatrix} I \\ G \end{bmatrix} K_{\mathcal{I}S}$ with $\|G\|_{\max} \leq 2$.*

Then

$$\begin{aligned} \|K_{XY} - UK_{\mathcal{I}Y}\|_{\max} &\leq \max_{\substack{x \in X \\ y \in Y}} \min_{v \in S} (|\kappa(x, y) - \kappa(x, v)| + \|K_{Xy} - K_{Xv}\|) \\ &\quad + 2r \max_{\substack{x \in \mathcal{I} \\ y \in Y}} \min_{v \in S} (|\kappa(x, y) - \kappa(x, v)| + \|K_{Xy} - K_{Xv}\|), \end{aligned} \quad (18)$$

where $r = \text{card}(\mathcal{I})$.

Proof. We decompose K_{XY} as

$$\begin{aligned} K_{XY} &= K_{XS}K_{XS}^+K_{XY} + E_1 \quad \text{with} \quad E_1 = K_{XY} - K_{XS}K_{XS}^+K_{XY} \\ &= P \begin{bmatrix} I \\ G \end{bmatrix} K_{\mathcal{I}S}K_{XS}^+K_{XY} + E_1 \\ &= P \begin{bmatrix} I \\ G \end{bmatrix} (K_{\mathcal{I}Y} + E_2) + E_1 \quad \text{with} \quad E_2 = K_{\mathcal{I}S}K_{XS}^+K_{XY} - K_{\mathcal{I}Y} \\ &= P \begin{bmatrix} I \\ G \end{bmatrix} K_{\mathcal{I}Y} + P \begin{bmatrix} I \\ G \end{bmatrix} E_2 + E_1. \end{aligned} \quad (19)$$

According to Corollary 2.1,

$$\|E_1\|_{\max} \leq \max_{\substack{x \in X \\ y \in Y}} \min_{v \in S} (|\kappa(x, y) - \kappa(x, v)| + \|K_{Xy} - K_{Xv}\|). \quad (20)$$

Similarly, for E_2 , we have

$$\|E_2\|_{\max} \leq \max_{\substack{x \in \mathcal{I} \\ y \in Y}} \min_{v \in S} (|\kappa(x, y) - \kappa(x, v)| + \|K_{Xy} - K_{Xv}\|). \quad (21)$$

Since $\|G\|_{\max} \leq 2$ and the row size of E_2 is equal to $r = \text{card}(\mathcal{I})$, it follows that

$$\|GE_2\|_{\max} \leq 2r\|E_2\|_{\max}.$$

Together with (21), (20), and (19), we deduce the inequality in (18). \square

The estimate in Theorem 3.2 relates the approximation error to the subset S . We show a more geometric characterization of the error bound of Theorem 3.2 in the following theorem. This theorem implies that the approximation error depends on the ability of S to capture Y , which is similar to the two-sided approximation case described in Theorem 2.3.

Theorem 3.3. *Let $X, Y, \kappa, S, \mathcal{I}$ be given in Theorem 3.2 and let $K_{XY} \approx UK_{\mathcal{I}Y}$ be the approximation in Theorem 3.2. Then*

$$\begin{aligned} \|K_{XY} - UK_{\mathcal{I}Y}\|_{\max} &\leq L(X \times Y, X \times S)\delta_{Y,S} + (1 + 2r)\sqrt{m}L(Y, S)_X\delta_{Y,S} \\ &\quad + 2rL(\mathcal{I} \times Y, \mathcal{I} \times S)\delta_{Y,S}, \end{aligned} \quad (22)$$

where $m = \text{card}(X)$, $r = \text{card}(\mathcal{I})$.

Proof. The proof is analogous to that of Theorem 2.3. According to (16), we deduce that

$$\begin{aligned} \max_{\substack{x \in X \\ y \in Y}} \min_{v \in S} (|\kappa(x, y) - \kappa(x, v)| + \|K_{Xy} - K_{Xv}\|) &\leq \max_{\substack{x \in X \\ y \in Y}} \min_{v \in S} (L(X \times Y, X \times S)|y - v| + \sqrt{m}L(Y, S)_X|y - v|) \\ &= \max_{\substack{x \in X \\ y \in Y}} (L(X \times Y, X \times S)\text{dist}(y, S) + \sqrt{m}L(Y, S)_X\text{dist}(y, S)) \\ &= L(X \times Y, X \times S)\delta_{Y,S} + \sqrt{m}L(Y, S)_X\delta_{Y,S}. \end{aligned}$$

Similarly, it can be deduced that

$$\max_{\substack{x \in \mathcal{I} \\ y \in Y}} \min_{v \in S} (|\kappa(x, y) - \kappa(x, v)| + \|K_{Xy} - K_{Xv}\|) \leq L(\mathcal{I} \times Y, \mathcal{I} \times S)\delta_{Y,S} + \sqrt{m}L(Y, S)_X\delta_{Y,S}.$$

Inserting the above two inequalities into (18) completes the proof. \square

From Theorem 3.3, it is easy to see that smaller $\delta_{Y,S}$ contributes to better approximation and the approximation error is zero if $S = Y$. Also, we see that the smoother the kernel function is (small Lipschitz constant), the more accurate the low-rank approximation will be. This is consistent with the fact that smooth kernel functions yield kernel matrices with rapidly decaying singular values.

Compared to the error estimates in Theorem 2.2 and Theorem 2.3 for the *two-sided* factorization, the estimates for the *one-sided* factorization in Theorem 3.2 and Theorem 3.3 appear to be better since they do not contain the norm of any matrix, for example, the possibly large factor $\|K_{S_1 S_2}^+\|$ in Theorem 2.2 and Theorem 2.3. This factor disappears when only *one* geometric selection is performed (for either rows or columns), as shown in Corollary 2.1 and Theorem 3.2.

3.3 The symmetric case

In this section, we consider a variant of the approximation (3) when the kernel matrix $K_{XX} = [\kappa(x, y)]_{x, y \in X}$ is associated with *one* set of points X and a symmetric kernel $\kappa(x, y)$. This type of kernel matrix arises frequently as covariance or correlation matrices in statistics and machine learning. In order to preserve the symmetry of K_{XX} , we compute a symmetric factorization of the form

$$K_{XX} \approx UK_{\mathcal{I}\mathcal{I}}U^T \quad \text{with } \mathcal{I} \subseteq X \quad (23)$$

whose structure-preserving properties are shown in the next proposition. This is the symmetric version of the “double-sided ID” [42].

Proposition 3.2. *If K_{XX} is symmetric, then the low-rank approximation $UK_{\mathcal{I}\mathcal{I}}U^T$ in (23) is also symmetric. If K_{XX} is assumed to be positive semi-definite, then $UK_{\mathcal{I}\mathcal{I}}U^T$ is also positive semi-definite.*

Proof. Since $\mathcal{I} \subseteq X$, $K_{\mathcal{I}\mathcal{I}}$ is a principal submatrix of K_{XX} . If K_{XX} is symmetric, $K_{\mathcal{I}\mathcal{I}}$ is also symmetric, which implies that $UK_{\mathcal{I}\mathcal{I}}U^T$ is symmetric.

If K_{XX} is positive semi-definite, then $K_{\mathcal{I}\mathcal{I}}$ is also positive semi-definite since it is a principal submatrix of K_{XX} . As a result, $UK_{\mathcal{I}\mathcal{I}}U^T$ is symmetric positive semi-definite. \square

The symmetric factorization in (23) is a straightforward extension of the one-sided factorization and the algorithm is summarized in Algorithm 3.

Algorithm 3 Data-driven compression of K_{XX} with one set of points X

Input: Dataset $X = \{x_1, \dots, x_n\} \subset \mathbb{R}^d$, kernel function κ , number of sample points r

Output: Low-rank approximation $K_{XX} \approx UK_{\mathcal{I}\mathcal{I}}U^T$

- 1: Apply a linear complexity geometric selection algorithm to X to generate r sample points S
- 2: Apply ID to the n -by- r kernel matrix K_{XS} :

$$K_{XS} = [\kappa(x, y)]_{\substack{x \in X \\ y \in S}} = P \begin{bmatrix} I \\ G \end{bmatrix} K_{\mathcal{I}S}, \quad (24)$$

where $\mathcal{I} \subseteq X$, P is a permutation matrix and $\|G\|_{\max} \leq 2$

3: Define $U = P \begin{bmatrix} I \\ G \end{bmatrix}$

4: **return** $U, K_{\mathcal{I}\mathcal{I}}$

4 Numerical experiments

In this section, we illustrate the data-driven geometric approach using both low- and high-dimensional data. All experiments were conducted in MATLAB R2021a on a MacBook Pro with Apple M1 chip and 8GB of RAM.

4.1 Data on a manifold in three dimensions

For data in low dimensional ambient space, e.g., $d = 3$, there exist several effective methods for compressing kernel matrices. However, their efficiency may decrease when the separation between the sets X and Y decreases and when the data lies on a manifold rather than be distributed relatively uniformly in the ambient space. To illustrate the advantages of the geometric approach in these cases, we use a sequence of three datasets as illustrated in Figure 4. In each dataset, X and Y each contain 1400 points. From Dataset 1 to 3, Y is a vertical shift of X by 2.7, 2, and 0.5, respectively. The minimum distance between points in X and points in Y from Datasets 1 to 3 is 1, 0.43, 0.12, respectively. The smallest bounding boxes for X and Y are well-separated in Dataset 1, adjacent in Dataset 2, and overlapping in Dataset 3. With these data, kernel matrices were constructed using the kernel function $\kappa(x, y) = 1/|x - y|$.

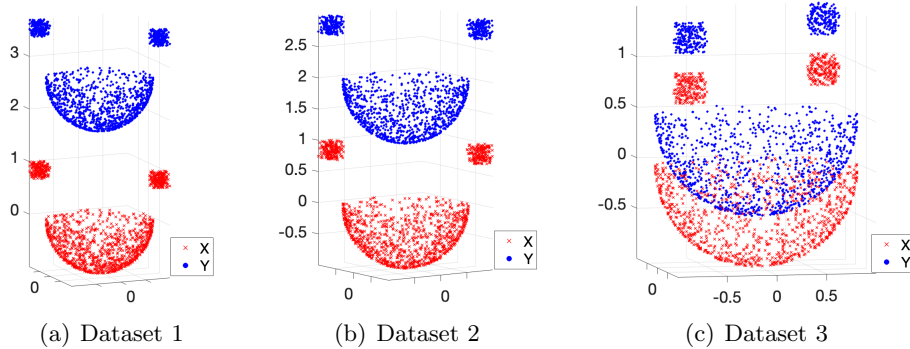


Figure 4: Sequence of three datasets in three dimensions. From Datasets 1 to 3, Y is a vertical shift of X by 2.7, 2, and 0.5, respectively. The minimum distance between points in X and points in Y from Dataset 1 to 3 is 1, 0.43, 0.12, respectively.

Test 1. Robustness with respect to data geometries. For above the settings, we compare the approximation error of the data-driven geometric approach with that of an algebraic method, ACA [8], and proxy point method (‘proxy’) [54]. For the data-driven method (‘DD’), we construct a one-sided factorization (Algorithm 2) using farthest point sampling with sample size at most $2r$ for a rank- r approximation. For the proxy point method, the sample size is 2000 for Ω_X (the smallest bounding box containing X) and 10000 for Ω_Y , independent of the approximation rank. Figure 5 shows, for the various methods, the relative matrix approximation error as a function of the rank of the approximation. The relative error is defined as $\|K - \tilde{K}\|/\|K\|$, where \tilde{K} denotes the low-rank approximation to K and $\|\cdot\|$ denotes the 2-norm. The optimal relative approximation error as computed by the SVD is also shown.

We observe that all methods are effective for Dataset 1, with the data-driven method - DD - being the most efficient and most closely tracking the SVD approximation error. We remark that the budget of points is not effectively used in proxy point method when the data is unstructured. Hence it is computationally more expensive than DD and ACA in this experiment.

For Dataset 2, we are at the boundary at which hybrid methods are effective, i.e., those methods that assume a separation of the bounding boxes for X and Y . However, DD and ACA still closely track the SVD approximation error.

For Dataset 3, the points in X and Y are actually “intermingled” (overlapping bounding boxes). ACA might not effectively sample X and Y in this dataset, especially since the dataset contains disjoint clusters (points on a half-shell and points in small cubes). However, DD continues to closely track the SVD approximation error.

4.2 Data in high-dimensional ambient space

The data-driven geometric approach can be efficient for data in high-dimensional ambient space, whereas many other existing low-rank compression methods have cost that is exponentially de-

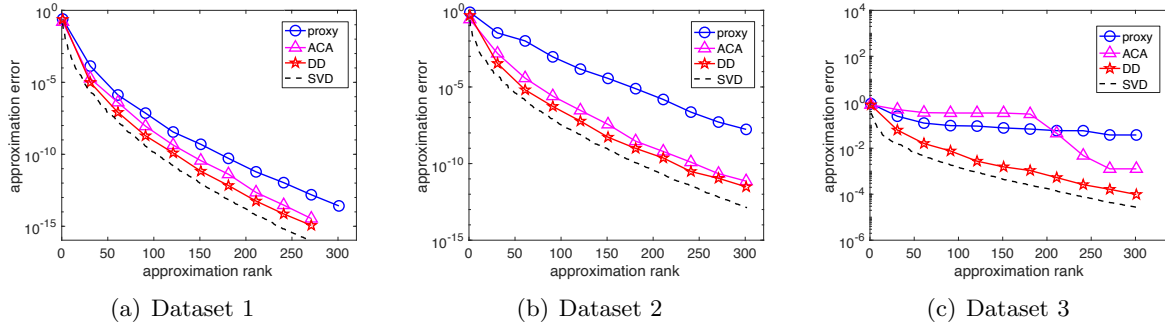


Figure 5: Accuracy comparison of different methods for constructing low-rank factorizations on the kernel matrices defined by Datasets 1, 2, and 3 shown in Figure 4 and the kernel function $\kappa(x, y) = 1/|x - y|$.

pendent on the dimensionality of ambient space. To demonstrate the data-driven approach for high-dimensional data, we use two datasets from the UCI machine learning repository:¹ Covertype ($n = 581,012$, $d = 54$) and Gas Sensor Array Drift ($n = 13,910$, $d = 128$). Each dataset is standardized to have mean zero and variance along each dimension equal to one. Instead of using the entire datasets, we choose X and Y to be two subsets of random samples, selected without replacement, with 8000 points for X and 10000 points for Y .

For both datasets, the kernel matrix K_{XY} is a 8000-by-10000 matrix associated with the Gaussian kernel $\kappa(x, y) = \exp(-|x - y|^2/\sigma^2)$. Since the bandwidth parameter σ controls the smoothness of the kernel, we consider σ from among three values, denoted as $\sigma_1, \sigma_2, \sigma_3$ and chosen to be 100%, 50%, 25% of the radius of X , respectively.

Test 2. Different geometric selection schemes. We first examine the effect of different geometric selection schemes (see Section 1) used to construct the two-sided low-rank factorization (2). It has been observed in [18] that the approximation error can be extremely large if the subset is not chosen properly. In this case, to deal with the pseudoinverse, a stable implementation proposed in [43] was used in [18]:

$$K_{XY} \approx (K_{XS_2} R_\epsilon^+) (Q^T K_{S_1Y}), \quad (25)$$

where $K_{S_1S_2} = QR$ is the QR factorization of $K_{S_1S_2}$ and R_ϵ is derived from R by truncating singular values smaller than ϵ in the SVD. It is also noted in [18] that the above stabilization is *not* needed if the subset is well-chosen, i.e. spread evenly over the data. To make a fair comparison of different selection schemes, the stabilization in (25) is used. Namely, in Algorithm 1, $K_{S_1S_2}$ is replaced with its truncated QR factors: Q and R_ϵ^+ .

For these experiments, we use the Gas Sensor dataset with a Gaussian kernel with $\sigma = \sigma_1 \approx 307.52$.

Figure 6 shows the low-rank approximation error (relative error as in Figure 5) vs. approximation rank when different geometric selection schemes are used. We compare the following schemes: anchor net (‘ANC’), farthest point sampling (‘FPS’), uniform random sampling (‘Unif’), as well as mixtures of uniform random sampling and FPS (some points are generated by FPS, the rest by random sampling). In the mixed scheme, random sampling is used to reduce the cost of FPS and we use the experiment to observe the effect of augmenting FPS samples with random samples. In these cases, the mixtures are denoted ‘mixed1’, ‘mixed2’, ‘mixed3’, for 5%, 10%, 50% FPS samples with the remainder of the samples selected by uniform random sampling. We observe that ANC and FPS perform similarly. These methods have a clear advantage over pure random sampling, suggesting that the data has structure to be exploited that is hidden from pure random sampling. However, random sampling can reduce the cost of a pure FPS method. The accuracy of ANC and FPS is attributed to the use of evenly spaced points. The generation of evenly distributed points is studied in discrepancy theory for the unit cube (cf. [44, 39]) and recently extended to general

¹<https://archive.ics.uci.edu/ml/index.php>

geometries using deep neural networks (cf. [13, 17]). We also note that the approximation error for ‘DD2-Unif’ does not improve after approximation rank about 50, creating the “flat” portion in the plot. In fact, this is due to the stabilization (25) that prevents the approximation error from “blowing up”.

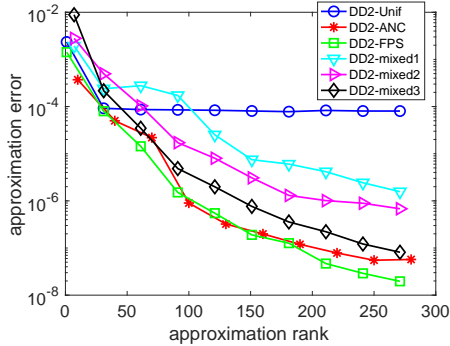


Figure 6: Accuracy comparison of different geometric selection schemes for constructing two-sided data-driven low-rank factorizations on the kernel matrix defined by the Gas Sensor dataset ($d = 128$) and a Gaussian kernel with the bandwidth $\sigma_1 \approx 307.5$.

Test 3. One-sided vs. two-sided low-rank factorization. With the same dataset and kernel as immediately above, we compared the approximation error for one-sided and two-sided low-rank factorization. Figure 7 shows these results. The one- and two-sided cases are denoted as ‘DD1’ and ‘DD2’, respectively, and each is tested with ‘Unif’, ‘ANC’, and ‘FPS’ geometric selection.

We observe that one-sided factorization is generally more accurate. This is consistent with the theoretical results in Theorem 2.2 and Theorem 3.2, where the two-sided approximation error estimate contains the norm of a pseudoinverse matrix while the one-sided approximation estimate doesn’t contain any matrix norm.

We notice again the stagnating accuracy for ‘DD2-Unif’ when the approximation rank is larger than 50. On the contrary, “DD1-Unif” gives effective error reduction as the approximation rank increases. The difference reveals the fact that the two-sided factorization is *not* as numerically stable as the one-sided factorization. It should be noted, however, that the one-sided factorization is more expensive to compute than the two-sided factorization. The one-sided factorization uses geometric selection on only X or only Y rather than both X and Y and applies algebraic compression to a much larger intermediate matrix than the two-sided factorization.

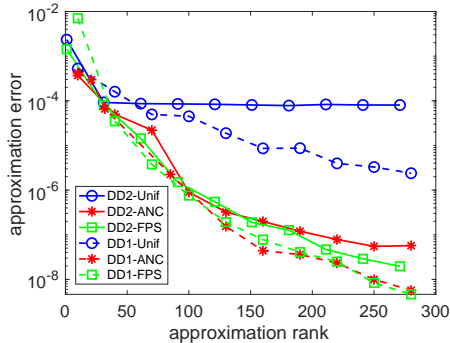


Figure 7: Accuracy comparison of one-sided vs. two-sided data-driven factorizations on the kernel matrix defined by the Gas Sensor dataset ($d = 128$) and a Gaussian kernel with the bandwidth $\sigma_1 \approx 307.5$.

Test 4. Comparison with ACA and robustness with respect to kernel parameters.

There exist a few low-rank compression algorithms that are both efficient in the high-dimensional case and able to handle intermingled data. One notable method is the ACA method [8], which

does not require access to the full kernel matrix, has linear complexity, and produces a one-sided factorization. We thus now compare the data-driven geometric approach with ACA. Specifically, we use the data-driven approach to compute a one-sided low-rank factorization with ANC and FPS geometric selection schemes, corresponding to “DD-ANC” and “DD-FPS” in Figures 8 to 10.

Figures 8 and 9 show the approximation errors for the Covertypes and Gas Sensor datasets, respectively, each with three values of bandwidth σ for the Gaussian kernel. For the Covertypes dataset, the data-driven methods yield much better accuracy than ACA for all choices of σ . The accuracy of ACA stagnates as the approximation rank is increased, suggesting that clusters in the dataset have prevented ACA from selecting rows and columns that help represent the kernel matrix.

For the Gas Sensor dataset, all methods behave similarly for a large bandwidth σ_1 . For a smaller bandwidth σ_3 , ACA displays stagnation in accuracy for approximation rank greater than 100. The smaller bandwidth makes the Gaussian kernel less smooth, and accentuates the effect of clusters in the data. These issues in ACA have been explored previously [10, 20]. In general, these issues reflect the challenge in approximating kernel matrices associated with high ambient dimensions but possibly lower dimensional structures within these dimensions.

Figure 10 shows timings for computing the low-rank approximations. Although our timings are limited to MATLAB execution, the results indicate that a geometric approach using a fast geometric selection scheme (e.g., ANC) can be faster than ACA for the same approximation error. The results also suggest that ANC is significantly faster than FPS.

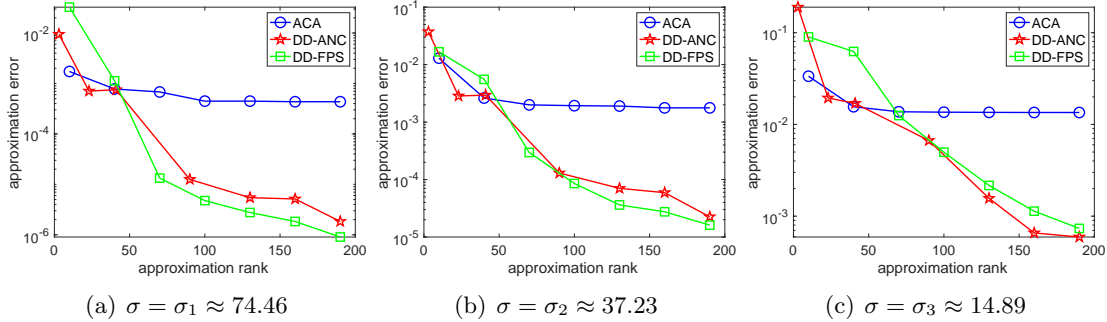


Figure 8: Accuracy comparison of one-sided data-driven factorizations (DD-ANC and DD-FPS) with ACA on kernel matrices defined by the Covertypes dataset ($d=54$) and Gaussian kernel with three different bandwidths σ .

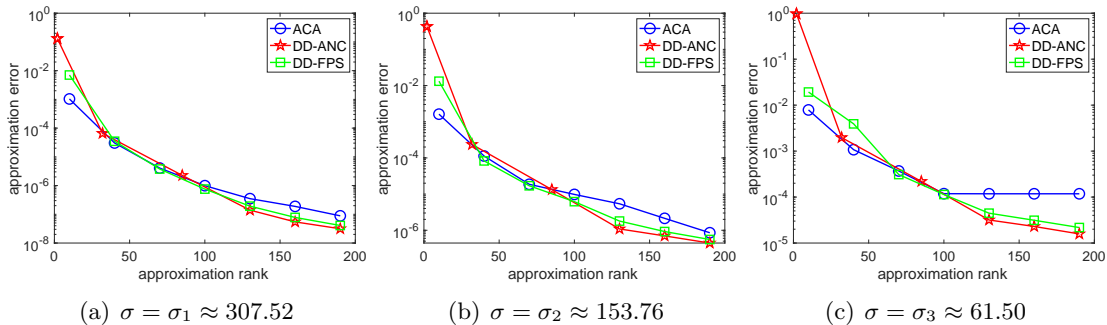


Figure 9: Accuracy comparison of one-sided data-driven factorizations (DD-ANC and DD-FPS) with ACA on the kernel matrices defined by the Gas Sensor dataset ($d=128$) and the Gaussian kernel with three different bandwidths σ .

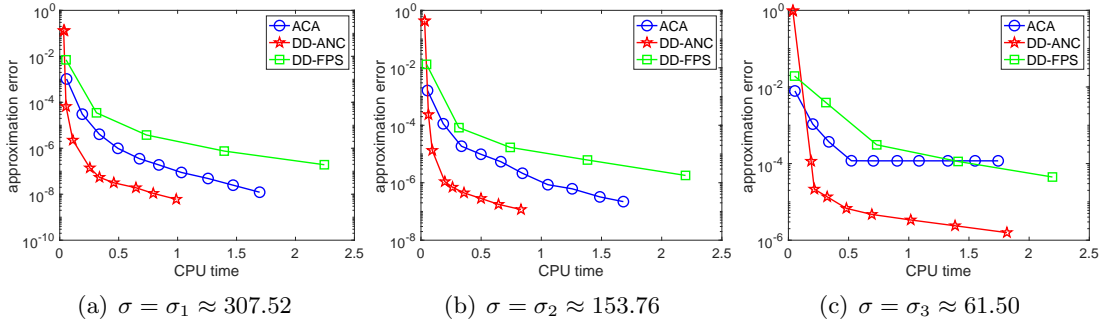


Figure 10: Time comparison of one-sided data-driven factorizations (DD-ANC and DD-FPS) with ACA on the kernel matrices defined by the Gas Sensor dataset ($d=128$) and the Gaussian kernel with three different bandwidths σ . CPU timings (in seconds) are the average of 10 runs.

4.3 Complexity test

In this section, we demonstrate the linear complexity of the proposed data-driven methods with respect to the size of the data.

Test 5. Linear complexity with respect to data size. We consider approximating an n -by- n kernel matrix K_{XY} with increasing matrix size n and dimension d . We consider dimensions $d = 3, 10, 50, 100$ and generate synthetic data X, Y in \mathbb{R}^d . X and Y are randomly sampled from the uniform distribution over $[0, 1]^d$ and $[2, 3]^d$, respectively. The kernel function is chosen as $\log|x - y|$. We use the one-sided factorization in Algorithm 2 based on farthest point sampling. In Figure 11, we report the peak memory use and timing for our method as n increases. The CPU time is computed as an average over ten repeated runs. For all cases in Figure 11, the relative low-rank approximation error is around 2×10^{-4} .

It is easily seen from Figure 11 that, for each dimension d , the peak memory and timing both increase approximately linearly as a function of n , i.e. the number of points in X or Y .

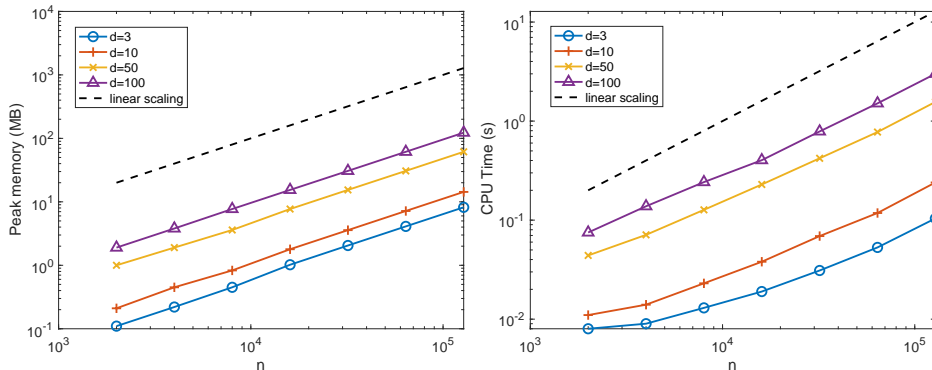


Figure 11: Linear scaling tests of the data-driven factorization method on the kernel matrices defined by the synthetic data X, Y sampled from the uniform distribution over $[0, 1]^d$ and $[2, 3]^d$, respectively, and the kernel function $\log|x - y|$. Left: peak memory use. Right: CPU time (average of 10 runs).

4.4 Kernel test

To show that the proposed data-driven approach can be applied to various kinds of kernel functions defined in high dimensions, we consider six different kernel functions (see Table 1) defined over a dataset in 561 dimensions. We demonstrate the generality and accuracy of the data-driven approach by comparing to ACA.

Table 1: Kernels used for experiment in Table 2. In κ_4 , the constant $c = \frac{0.8}{\max_{x \in X, y \in Y} |x-y|^2}$, and in κ_5 , x_1 denotes the first entry of the vector $x \in \mathbb{R}^d$

$\kappa_1(x, y)$	$\kappa_2(x, y)$	$\kappa_3(x, y)$	$\kappa_4(x, y)$	$\kappa_5(x, y)$	$\kappa_6(x, y)$
$ x - y $	$\log x - y $	$\left(1 + \left \frac{x-y}{R}\right ^2\right)^{-1}$	$\exp\left(-\frac{1}{1-c x-y ^2}\right)$	$\frac{x_1}{ x - y }$	$x \cdot y + (x \cdot y)^2 + (x \cdot y)^3$

Test 6. Approximating various types of kernel functions. We use a high dimensional dataset from the UCI Machine Learning Repository: *Smartphone Dataset for Human Activity Recognition in Ambient Assisted Living*². The training data contains $n = 4252$ instances with $d = 561$ attributes. We choose X to be the standardized data, and define $Y = \frac{2R}{\sqrt{d}} + X$, where $R = \max_{x \in X} \text{dist}(x, 0)$. By construction, X and Y do not overlap and kernel functions in Table 1 are all well-defined over $X \times Y$.

The kernel functions $\kappa_1(x, y), \dots, \kappa_6(x, y)$ in the experiment are given in Table 1.

In Table 2, we report the relative approximation error $\|K - UV\|/\|K\|$ with respect to the approximation rank r , which is equal to the number of columns of U . Three methods are compared: ACA, the data-driven compression in Algorithm 2 with farthest point sampling (“DD-FPS”) or anchor net method (“DD-ANC”).

We see from Table 2 that DD-ANC achieves the best result for all kernels and ranks tested. For the same approximation rank r , the accuracy of DD-ANC is noticeably higher than that of DD-FPS and ACA. DD-FPS outperforms ACA for almost all cases except $\kappa_4(x, y)$ when $r = 10, \dots, 170$. Together with Test 4 in Section 4.2, the results show that the proposed linear complexity data-driven approach is not only more robust, but also more accurate for the high dimensional dataset with general kernels. Compared to existing methods, one advantage of the data-driven method is that, for the same dataset and fixed rank r , the geometric selection is performed only *once* and can be used for different kernel functions or kernel function parameters. This can hardly be achieved by methods that require kernel function evaluation as the first step of the compression. For example, for algebraic methods such as ICA and ACA, if the kernel function changes, the pivots need to be computed anew. In Table 2, for each r , ACA computes pivots six times for six kernels, while DD-FPS and DD-ANC each only select one subset, which is used for all six kernel functions.

5 Conclusion

For compressing low-rank kernel matrices where sets of points X and Y are available, it appears appealing to use subsets of X and Y that capture the geometry of X and Y . This paper presented theoretical justification and numerical tests that argue for choosing points such that no original point in X (or Y) is very far from a point chosen for the subset. If these subsets can be selected in linear time, then the overall compression algorithm can be performed in linear time, which is optimal for kernel matrices. We demonstrated effective low-rank compression for both low and high dimensional datasets using geometric selection based on farthest point sampling and the anchor net method, which are both linear scaling. It is possible that even more sophisticated linear scaling schemes for selecting subsets can lead to even better approximation accuracy with the same number of selected points, especially in the high-dimensional case.

References

- [1] M. Ainsworth and T. Vejchodský. Fully computable robust a posteriori error bounds for singularly perturbed reaction–diffusion problems. *Numerische Mathematik*, 119(2):219–243,

²<https://archive.ics.uci.edu/ml/machine-learning-databases/00364/>

Table 2: Rank- r approximation accuracy of the data-driven factorizations (DD-ANC and DD-FPS) and ACA on the kernel matrices defined by the Smartphone Dataset ($d = 561$) and six kernel functions shown in Table 1.

r		10	50	90	130	170	210	250
$\kappa_1(x, y)$	ACA	2.4E-3	4.8E-4	1.2E-4	8.2E-5	3.1E-5	1.7E-5	8.5E-6
	DD-FPS	1.3E-3	2.4E-4	1.4E-4	4.2E-5	3.5E-5	1.4E-5	4.7E-6
	DD-ANC	3.5E-4	9.0E-5	3.8E-5	1.9E-5	9.9E-6	4.6E-6	2.7E-6
$\kappa_2(x, y)$	ACA	2.2E-4	6.1E-5	4.8E-5	2.3E-5	6.7E-6	3.6E-6	2.7E-6
	DD-FPS	1.7E-4	4.5E-5	2.7E-5	7.5E-6	5.1E-6	2.4E-6	1.1E-6
	DD-ANC	5.9E-5	1.6E-5	6.4E-6	3.6E-5	1.9E-6	9.0E-7	5.5E-7
$\kappa_3(x, y)$	ACA	2.5E-3	9.3E-4	3.2E-4	1.8E-4	6.3E-5	4.3E-5	2.9E-5
	DD-FPS	5.2E-3	9.8E-4	2.5E-4	1.2E-4	6.8E-5	3.8E-5	2.0E-5
	DD-ANC	8.3E-4	1.3E-4	6.4E-5	3.9E-5	1.8E-5	9.9E-6	6.0E-6
$\kappa_4(x, y)$	ACA	1.2E-2	8.7E-4	3.3E-4	1.4E-4	7.1E-5	4.9E-5	4.8E-5
	DD-FPS	3.6E-2	2.5E-3	3.9E-4	1.7E-4	1.0E-4	4.6E-5	1.8E-5
	DD-ANC	1.8E-3	2.8E-4	1.2E-4	6.2E-5	3.5E-5	1.7E-5	9.0E-6
$\kappa_5(x, y)$	ACA	9.1E-4	1.7E-4	7.7E-5	5.7E-5	2.2E-5	1.1E-5	7.1E-6
	DD-FPS	4.0E-4	1.1E-4	4.9E-5	2.1E-5	1.1E-5	4.1E-6	2.1E-6
	DD-ANC	2.9E-4	5.7E-5	3.2E-5	1.3E-5	5.4E-6	2.0E-6	1.2E-6
$\kappa_6(x, y)$	ACA	1.3E-1	8.9E-3	5.1E-3	2.8E-3	2.2E-3	1.8E-3	1.7E-3
	DD-FPS	1.8E-2	3.7E-3	2.0E-3	1.2E-3	9.8E-4	7.6E-4	6.3E-4
	DD-ANC	1.2E-2	2.7E-3	1.1E-3	7.5E-4	6.8E-4	5.4E-4	4.5E-4

- 2011.
- [2] C. R. Anderson. An implementation of the fast multipole method without multipoles. *SIAM J. Sci. Statist. Comput.*, 13(4):923–947, 1992.
 - [3] David Anderson, Simon Du, Michael Mahoney, Christopher Melgaard, Kunming Wu, and Ming Gu. Spectral gap error bounds for improving CUR matrix decomposition and the Nyström method. In *Artificial Intelligence and Statistics*, pages 19–27, 2015.
 - [4] K. E. Atkinson. The numerical solution of the eigenvalue problem for compact integral operators. *Transactions of the American Mathematical Society*, 129(3):458–465, 1967.
 - [5] J. Barnes and P. Hut. A hierarchical $O(N \log N)$ force-calculation algorithm. *Nature*, 324:446–449, December 1986.
 - [6] M. Bauer, M. Bebendorf, and B. Feist. Kernel-independent adaptive construction of \mathcal{H}^2 -matrix approximations, 2020.
 - [7] M. Bebendorf. Approximation of boundary element matrices. *Numer. Math.*, 86(4):565–589, 2000.
 - [8] M. Bebendorf and S. Rjasanow. Adaptive low-rank approximation of collocation matrices. *Computing*, 70(1):1–24, 2003.
 - [9] Christopher M. Bishop. *Pattern Recognition and Machine Learning*. Springer, 2006.
 - [10] S. Börm and L. Grasedyck. Hybrid cross approximation of integral operators. *Numer. Math.*, 101(2):221–249, 2005.
 - [11] S. Börm, L. Grasedyck, and W. Hackbusch. Introduction to hierarchical matrices with applications. *Eng. Anal. Bound. Elem.*, 27(5):405–422, 2003.
 - [12] D. Braess and J. Schöberl. Equilibrated residual error estimator for edge elements. *Mathematics of Computation*, 77(262):651–672, 2008.
 - [13] D. Cai. Physics-informed distribution transformers via molecular dynamics and deep neural networks. *Journal of Computational Physics*, 468:111511, 2022.
 - [14] D. Cai and Z. Cai. A hybrid a posteriori error estimator for conforming finite element approximations. *Computer Methods in Applied Mechanics and Engineering*, 339:320 – 340, 2018.
 - [15] D. Cai, Z. Cai, and S. Zhang. Robust equilibrated a posteriori error estimator for higher order finite element approximations to diffusion problems. *Numerische Mathematik*, 144(1):1–21, 2020.
 - [16] D. Cai, E. Chow, L. Erlandson, Y. Saad, and Y. Xi. SMASH: Structured matrix approximation by separation and hierarchy. *Numerical Linear Algebra with Applications*, 25(6):e2204, 2018.
 - [17] D. Cai, Y. Ji, H. He, Q. Ye, and Y. Xi. AUTM Flow: Atomic Unrestricted Time Machine for Monotonic Normalizing Flows. In *Proceedings of the Thirty-Eighth Conference on Uncertainty in Artificial Intelligence*, volume 180, pages 266–274. PMLR, 2022.
 - [18] D. Cai, J. Nagy, and Y. Xi. Fast deterministic approximation of symmetric indefinite kernel matrices with high dimensional datasets. *SIAM Journal on Matrix Analysis and Applications*, 43(2):1003–1028, 2022.
 - [19] D. Cai and P. S. Vassilevski. Eigenvalue problems for exponential-type kernels. *Computational Methods in Applied Mathematics*, 20(1):61–78, 2020.
 - [20] Léopold Cambier and Eric Darve. Fast low-rank kernel matrix factorization using skeletonized interpolation. *SIAM Journal on Scientific Computing*, 41(3):A1652–A1680, 2019.
 - [21] Hongwei Cheng, Zydrunas Gimbutas, Per-Gunnar Martinsson, and Vladimir Rokhlin. On the compression of low rank matrices. *SIAM Journal on Scientific Computing*, 26(4):1389–1404, 2005.
 - [22] E. Chow and Y. Saad. Preconditioned Krylov subspace methods for sampling multivariate Gaussian distributions. *SIAM J. Sci. Comput.*, 36(2):A588–A608, 2014.

- [23] A. Cortinovis and D. Kressner. Low-rank approximation in the frobenius norm by column and row subset selection. *SIAM Journal on Matrix Analysis and Applications*, 41(4):1651–1673, 2020.
- [24] Yuval Eldar, Michael Lindenbaum, Moshe Porat, and Yehoshua Y Zeevi. The farthest point strategy for progressive image sampling. *IEEE Transactions on Image Processing*, 6(9):1305–1315, 1997.
- [25] L. Erlandson, D. Cai, Y. Xi, and E. Chow. Accelerating parallel hierarchical matrix-vector products via data-driven sampling. In *2020 IEEE International Parallel and Distributed Processing Symposium (IPDPS)*, pages 749–758, 2020.
- [26] Adrianna Gillman, Patrick M. Young, and Per-Gunnar Martinsson. A direct solver with $o(n)$ complexity for integral equations on one-dimensional domains. *Frontiers of Mathematics in China*, 7(2):217–247, 2012.
- [27] Sergei A Goreinov and Eugene E Tyrtyshnikov. The maximal-volume concept in approximation by low-rank matrices. *Contemporary Mathematics*, 280:47–52, 2001.
- [28] Sergei A Goreinov and Eugene E Tyrtyshnikov. Quasioptimality of skeleton approximation of a matrix in the Chebyshev norm. In *Doklady Mathematics*, volume 83, pages 374–375. Springer, 2011.
- [29] L. Greengard and V. Rokhlin. A fast algorithm for particle simulations. *J. Comput. Phys.*, 73:325–348, 1987.
- [30] M. Gu and S. C. Eisenstat. Efficient algorithms for computing a strong rank-revealing QR factorization. *SIAM J. Sci. Comput.*, 17(4):848–869, 1996.
- [31] W. Hackbusch. *Hierarchical Matrices: Algorithms and Analysis*. Springer Series in Computational Mathematics. Springer Berlin Heidelberg, 2015.
- [32] W. Hackbusch, B.N. Khoromskij, and S.A. Sauter. On \mathcal{H}^2 -matrices. In Hans-Joachim Bungartz, Ronald H. W. Hoppe, and Christoph Zenger, editors, *Lectures on Applied Mathematics*, pages 9–29. Springer, Berlin, 2000.
- [33] Wolfgang Hackbusch and Zenon Paul Nowak. On the fast matrix multiplication in the boundary element method by panel clustering. *Numerische Mathematik*, 54(4):463–491, 1989.
- [34] H. He, J. Henderson, and J.C. Ho. Distributed tensor decomposition for large scale health analytics. In *The World Wide Web Conference*, pages 659–669, 2019.
- [35] H. He, Y. Xi, and J.C. Ho. Fast and accurate tensor decomposition without a high performance computing machine. In *2020 IEEE International Conference on Big Data (Big Data)*, pages 163–170. IEEE, 2020.
- [36] J. Henderson, H. He, B.A. Malin, J.C. Denny, A.N. Kho, J. Ghosh, and J.C. Ho. Phenotyping through semi-supervised tensor factorization (psst). In *AMIA Annual Symposium Proceedings*, volume 2018, page 564. American Medical Informatics Association, 2018.
- [37] G. C. Hsiao and W. L. Wendland. *Boundary integral equations*. Applied Mathematical Sciences. Springer, Berlin, Heidelberg, 2008.
- [38] R. Kress. *Linear Integral Equations*. Applied Mathematical Sciences. Springer New York, 2013.
- [39] L. Kuipers and H. Niederreiter. *Uniform distribution of sequences*. Courier Corporation, 2012.
- [40] WR Madych and SA Nelson. Bounds on multivariate polynomials and exponential error estimates for multiquadric interpolation. *Journal of Approximation Theory*, 70(1):94–114, 1992.
- [41] Michael W. Mahoney and Petros Drineas. CUR matrix decompositions for improved data analysis. *Proceedings of the National Academy of Sciences*, 106(3):697–702, 2009.
- [42] Per-Gunnar Martinsson and Joel A. Tropp. Randomized numerical linear algebra: Foundations and algorithms. *Acta Numerica*, 29:403–572, 2020.
- [43] Yuji Nakatsukasa. Fast and stable randomized low-rank matrix approximation. *arXiv preprint arXiv:2009.11392*, 2020.

- [44] H. Niederreiter. *Random number generation and quasi-Monte Carlo methods*. SIAM, 1992.
- [45] Gabriel Peyré and Laurent D Cohen. Geodesic remeshing using front propagation. *International Journal of Computer Vision*, 69(1):145–156, 2006.
- [46] V. Rokhlin. Rapid solution of integral equations of classical potential theory. *Journal of Computational Physics*, 60(2):187–207, 1985.
- [47] Thomas Schlömer, Daniel Heck, and Oliver Deussen. Farthest-point optimized point sets with maximized minimum distance. In *Proceedings of the ACM SIGGRAPH Symposium on High Performance Graphics*, pages 135–142, 2011.
- [48] X. Sun and N.P. Pitsianis. A matrix version of the fast multipole method. *SIAM Rev.*, 43(2):289–300, 2001.
- [49] E. Tyrtshnikov. Mosaic-skeleton approximations. *CALCOLO*, 33(1):47–57, Jun 1996.
- [50] Vladimir Vapnik. *The Nature of Statistical Learning Theory*. Springer, 2013.
- [51] R. Verfürth. A posteriori error estimation and adaptive mesh-refinement techniques. *Journal of Computational and Applied Mathematics*, 50(1):67 – 83, 1994.
- [52] R. Verfürth. Robust a posteriori error estimates for stationary convection-diffusion equations. *SIAM Journal on Numerical Analysis*, 43(4):1766–1782, 2005.
- [53] Christopher KI Williams and Matthias Seeger. Using the Nyström method to speed up kernel machines. In *Advances in Neural Information Processing Systems*, pages 682–688, 2001.
- [54] X. Xing and E. Chow. Interpolative decomposition via proxy points for kernel matrices. *SIAM Journal on Matrix Analysis and Applications*, 41(1):221–243, 2020.
- [55] Zixi Xu, Léopold Cambier, François-Henry Rouet, Pierre L’Eplatennier, Yun Huang, Cleve Ashcraft, and Eric Darve. Low-rank kernel matrix approximation using skeletonized interpolation with endo-or exo-vertices. *arXiv preprint arXiv:1807.04787*, 2018.
- [56] O.C. Zienkiewicz and J.Z. Zhu. A simple error estimator and adaptive procedure for practical engineering analysis. *International Journal for Numerical Methods in Engineering*, 24(2):337–357, 1987.